RSC Advances

ROYAL SOCIETY OF CHEMISTRY

www.rsc.org/advances

Journal Name

RSCPublishing

ARTICLE

Block Copolymer-Cyclodextrin Supramolecular Assemblies as Soft Templates for the Synthesis of Titania Materials with Controlled Crystallinity, Porosity and Photocatalytic Activity

Cite this: DOI: 10.1039/x0xx00000x

Received 00th June 2014,
Accepted 00th August 2014

DOI: 10.1039/x0xx00000x

www.rsc.org/

Anthony Lannoy,[a] Rudina Bleta,*[a] Cécile Machut,[a] Eric Monflier[a] and Anne Ponchel[a]

Nanostructured titania materials with tunable porosity and crystalline framework were prepared in aqueous phase by using a template-directed colloidal self-assembly strategy. The approach employs the supramolecular assemblies formed between the randomly methylated β-cyclodextrin and the block copolymer P123 as soft templates and the sol-gel synthesised TiO_2 nanocrystals as building blocks. By combining X-ray diffraction, N_2-adsorption, field emission scanning electron microscopy and UV-visible spectroscopy, we show that considerable control over crystallite size, polymorph content and particle morphology could be achieved by using a delicate balance between the composition and structure of the supramolecular template as well as the reaction conditions. The photocatalytic activity of these mesoporous TiO_2 materials was evaluated in the photodegradation of a toxic herbicide, the phenoxyacetic acid (PAA), and was correlated to the structural and textural characteristics of the photocatalyst.

Introduction

Molecular self-assembly and supramolecular templating approaches have attracted a great deal of interest during the last twenty years owing to their ability to generate a wide variety of ordered organic, inorganic and hybrid nanostructures with tailored framework composition, pore structure, pore size, morphology and surface properties.[1-3] Since the discovery of the mesoporous silica of the M41S family,[4,5] many different strategies utilising supramolecular architectures as templates have been developed to prepare advanced materials with a variety of applications in many emerging fields ranging from biotechnology, to catalysis, energy storage, optics, molecular separation technology, etc.[6] Particularly, the template-directed colloidal self-assembly approach, utilising presynthesised colloidal nanocrystals as building blocks for the construction of nanostructured networks around a supramolecular template, has emerged as an important strategy to help fabricating nanostructures with high thermal stability and well-defined crystalline framework.[7-13] The structure and dimensions of both the template and the colloidal nanocrystals determine the characteristics of the final material.

As an important metal oxide semiconductor with numerous applications of fundamental and industrial interest, titanium dioxide (TiO_2) has attracted an immense attention since its commercial production in the early 20th century.[14] Besides its wide use as inorganic pigment in paints, titania has also been applied as one of the most efficient photocatalyst for the degradation of organic pollutants[15,16] and photocatalytic dissociation of water for hydrogen production.[17-19] Today, the importance of titania in the field of materials science is undeniable, as attested by the huge number of research publications, patents and citations produced each year.

TiO_2 commonly crystallises in three polymorphic forms, *i.e.* anatase (tetragonal, $I4_1/amd$), brookite (orthorhombic, *Pbca*) and rutile (tetragonal, $P4_2/mnm$). Among the three polymorphs, anatase and rutile have received the greatest attention due to the facility of their synthesis. Anatase has a band gap of 3.2 eV with the absorption edge at 386 nm which lies in the near UV range, whereas rutile has a lower band gap of 3.02 eV with the adsorption edge in the visible range at 416 nm. The anatase polymorph is usually reported to be more active than rutile,[20,21] mainly because of the fast electron-hole recombination in the latter resulting from its lower band gap.[22] Under controlled conditions, several authors[23-25] also succeeded in synthesising high crystalline pure brookite which was revealed to be very active in the photocatalytic hydrogen production.[25] Moreover, as demonstrated in several studies, TiO_2 photocatalysts

composed of mixed phases, usually exhibit superior activity compared to pure polymorphs due to the triggering of the electron and hole transfer between the different phases.[25-28]

It is today well-accepted that the photocatalytic reactions mainly take place on the surface of the irradiated semiconductor.[29] Consequently, in addition to the effect of the crystal phase composition mentioned above, other factors such as crystallite size, surface area, pore volume, adsorption properties of the pollutant and orientation of the active faces are also likely to affect the photocatalytic activity.[30-35]

To enhance crystallinity, titania is usually subjected to high thermal treatment temperatures during which the crystallites of metastable anatase and brookite, coarsen, grow and then transform to rutile when a critical size is reached.[36] Such phase transformation of nanocrystalline anatase and brookite to rutile is non-reversible due to the greater thermodynamic stability of the latter polymorph which generally provokes a deterioration of the framework and sometimes a complete collapse of the nanostructure.[37,38]

To avoid the aforementioned scenario, one strategy may consist in utilising template-assisted syntheses. So far, a large variety of soft and hard templates have been explored generating materials with tuned porosity and high thermal stability. [7,39-44] Among the soft templates, cyclodextrins are of great interest owing to their multifunctional properties, such as the formation of supramolecular adducts or host-guest inclusion complexes with a large number of molecules of appropriate size and shape.[45,46] Although the possibility of utilising cyclodextrins or supramolecular assemblies formed between block copolymers and cyclodextrins as templates to direct the synthesis of hierarchically structured porous silica[47-50] and alumina[51,52] has been explored so far, there is a limited number of reports devoted to titania.[53,54]

In a recent study,[51] we have shown that the randomly methylated β-cyclodextrin (RAMEB), where methylation occurs at the C2, C3 or C6 positions with statistically 1.8 OH groups modified per glucopyranose unit, can significantly affect the self-assembly of the amphiphilic block copolymer P123 in water by locating at the PEO-PPO interface layer, inducing a transition from spherical to ellipsoidal shape micelles. Interestingly, the RAMEB-P123 supramolecular assemblies were shown to act as efficient templates for tuning the porosity of alumina while promoting the formation of particles with a fiberlike morphology.

In the present study, we have undertaken a detailed investigation of the effect of these supramolecular assemblies on the porosity, crystallinity and photocatalytic activity of mesoporous titania materials prepared using a colloidal self-assembly approach. The characteristics of these materials will be described together with the results obtained on the photocatalytic degradation of the phenoxyacetic acid (PAA), a widely utilised herbicide, frequently detected in natural water.[55,56]

2. Experimental

Chemicals. The PEO-PPO-PEO triblock copolymer [PEO = poly(ethylene oxide) and PPO = poly(propylene oxide)], denoted Pluronic P123, was purchased from Sigma Aldrich. It has an average composition of $PEO_{20}PPO_{70}PEO_{20}$ and a molar weight of 5800 g/mol. Randomly methylated β-cyclodextrin (denoted RAMEB with an average degree of molar substitution, (DS) of 1.8 and average Mw 1310 g/mol) was a gift from Wacker Chemie GmbH. Titanium isopropoxyde, $Ti(O^iPr)_4$ (Mw 284.3 g/mol, d 0.96 g/cm^3), nitric acid (HNO_3, 68%) and phenoxyacetic acid (PAA, Mw 152.15 g/mol) were procured from Sigma Aldrich. All chemicals were used as received without further purification.

Synthesis of Titania Sols. Titanium dioxide nanoparticles were synthesised according to a previously reported sol-gel method.[41,57] Typically, in a 250 mL flask, 30 mL (0.1 mol) of $Ti(O^iPr)_4$ was dissolved in 27 mL (0.35 mol) of isopropanol. Then, 160 mL of hot distilled water was added rapidly at 85 °C under vigorous stirring at a hydrolysis ratio of h = $[H_2O]/[Ti]$ = 88. After 15 min, 1.3 mL of nitric acid ($[HNO_3]/[Ti]$ = 0.2) was added dropwise to peptise the hydroxide precipitate. The mixture was maintained under reflux at 85 °C for 16 h. The final product was a stable translucent suspension of titanium dioxide nanoparticles.

In parallel, 10 mL aliquots of micellar solution containing 7.8 wt % Pluronic P123 (P123/Ti molar ratio = 0.027) and various amounts of RAMEB (RAMEB/Ti molar ratio = 0.046-0.305) were mixed with 10 mL aliquots of the titania sol. The mixtures were stirred for 30 minutes then allowed to equilibrate at room temperature for 24 hours. Xerogels were recovered after drying the samples by evaporation at 60 °C for 48 h, after which time they were calcined in air at 500 °C for 2 h using a heating ramp of 5 °C/min. The final mesoporous materials were identified according to the following notation: Px-RBy where x and y represent the P123/Ti and RAMEB/Ti molar ratios respectively multiplied by 1000. For example, P27RB46 indicates a mesoporous titania prepared using a P123/Ti molar ratio of 0.027 and a RAMEB/Ti molar ratio of 0.046 whereas P27 indicates a mesoporous titania prepared with a P123/Ti molar ratio of 0.027 and without RAMEB. In some experiments, titania materials were calcined at 400 °C (16 h), 600 °C (2 h), 700 °C (2 h) and 800 °C (2 h) in order to follow the transformation sequence among the different polymorphs.

Characterisation Methods. *Powder X-ray diffraction* data were collected on a Siemens D5000 X-ray diffractometer in a Bragg-Brentano configuration with a Cu Kα radiation source. Scans were run over the angular domains $10° < 2\theta < 60°$ with a step size of 0.02° and a step time of 2 s. Crystalline phases were identified by comparing the experimental diffraction patterns to Joint Committee on Powder Diffraction Standards (JCPDS) files for anatase, brookite, and rutile. The refinement of the diffractograms was performed using the FullProf software[58] and its graphical interface WinPlotr.[59] Because of the numerous brookite reflections and the strong overlap of the diffraction lines, profile matching refinement was used to determine unit

cell parameters, background, peak shape, and zero shift. The quality of the fit was determined visually by inspection of the difference plot and statistically by the goodness of fit (χ^2) defined by:

$$\chi^2 = \sum w_i(y_{io} - y_{ic})^2/(N - P)$$

where w_i is the weight assigned to each observation, y_{io} and y_{ic} are the observed and calculated intensities, respectively, at the i^{th} step, N is the number of points used in the refinement and P is the number of least-squares parameters refined. The refinement was considered satisfactory when χ^2 was less than 4. The average crystallite size D was calculated from the Scherrer formula,[60] $D = K\lambda/(\beta \cos \theta)$, where K is the shape factor (a value of 0.9 was used in this study, considering that the particles are spherical), λ is the X-ray radiation wavelength (1.54056 Å for Cu Kα), β is the full width at half-maximum (fwhm) and θ is the Bragg angle. In addition, Rietveld refinements over a shorter 2θ range of 20-35° were also performed to determine the content of each polymorph. In this mode of refinement, only the scale factor was allowed to vary. Typical results obtained from profile matching and Rietveld refinements are shown in Fig. S1, ESI.

Nitrogen adsorption-desorption isotherms were collected at -196 °C using an adsorption analyser Micromeritics Tristar 3020. Prior to analysis, 200-400 mg samples were outgassed at 320 °C overnight to remove the species adsorbed on the surface. From N_2 adsorption isotherms, specific surface areas were determined by the BET method[61] and pore size distributions were calculated using the NLDFT (nonlocal density functional theory) model[62] assuming a cylindrical pore structure. The relative errors were estimated to be the following: S_{BET}, 5%; pore volume (pv) (DFT), 5%; pore size (ps) (DFT), 20%.

Field emission scanning electron microscopy (FE-SEM) observations were performed to examine the morphology of the samples using a FEG Hitachi S-4700 field-emission microscope operating at 5 kV. Before imaging, samples were covered with a thin layer of carbon to reduce the accumulation of charges at high magnification.

UV-visible diffuse reflectance spectra were collected using a Perkin Elmer Lambda 19 UV-Vis NIR spectrometer. $BaSO_4$ was used as the reference. The band gap energies (E_g) were calculated using the equation $E_g = (1239/\lambda)$ eV where λ is the wavelength in nm.

Attenuated Total Reflection Fourier Transform Infrared (ATR-FTIR) measurements were carried out on a Shimadzu IR Prestige-21 spectrometer equipped with a MIRacle Diamond prism. Spectra were recorded in the 4000-500 cm^{-1} region with a spectral resolution of 2 cm^{-1}.

The photocatalytic efficiency of the titania materials was evaluated in the photodegradation of the phenoxyacetic acid (PAA).[63,64] The experiments were carried out using a Pyrex cylindrical reactor equipped with a quartz window for the entrance of the UV irradiation. In a typical experiment, 50 mg photocatalyst (0.25 g/L) was introduced to a 0.15 g/L PAA solution and was maintained under stirring in the dark for 30 minutes to establish the adsorption-desorption equilibrium. Then, UV irradiation was performed using a 6 W UV lamp (Helios Italquartz, Italy) with a maximum emission at 352 nm. Aliquots were centrifuged at regular interval time and the substrate concentration in the supernatant was determined by high liquid performance liquid chromatography (HPLC, Perkin Elmer) analyses. The column used was a Perkin Elmer, Pecosphere C18 (83 mm length x 4.6 mm diameter). A mixture of acetonitrile (85 %, v/v) and deionised water (15 %, v/v) acidified with 0.2 % acetic acid was used as the mobile phase at a flow rate of 1.5 mL/min. Aliquots of 10 µL of the sample were injected and analysed at a wavelength of 360 nm using a photodiode array detector. The PAA degradation rate, given in percentage, refers to the difference in the PAA concentration before irradiation (C_0) and after 7 hours of irradiation (C_{7h}) divided by the PAA concentration before irradiation, *i.e.* 100 $(C_0-C_{7h})/C_0$.

3. Results and discussion

3.1 Effect of addition of RAMEB-P123 supramolecular assemblies

Taking advantage of the ability of the randomly methylated β-cyclodextrin to control the growth rate of block copolymer micelles, the RAMEB-P123 supramolecular assemblies were employed as soft templates for preparing a series of mesoporous titania materials with tunable structural and textural properties. Accordingly, a two-step synthesis procedure was applied, as schematised in Fig. 1.[41,51]

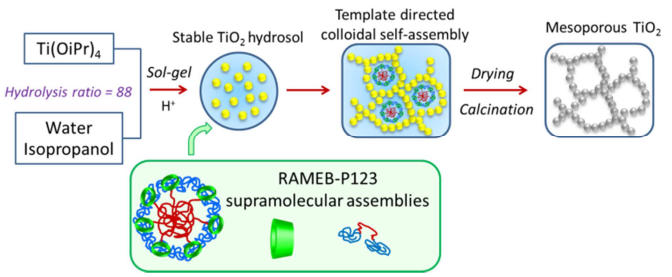

Fig. 1 Schematic illustration of the template-directed synthesis of mesoporous crystalline titania where TiO_2 colloids act as building blocks for the construction around the organic template of a nanostructured framework.

In a first step, a translucent hydrosol made-up of crystalline titania nanoparticles was synthesised in water/isopropanol solution (H_2O/Ti = 88) by a sol-gel method using titanium isopropoxide ($Ti(O^iPr)_4$) as inorganic precursor and nitric acid as peptising agent (HNO_3/Ti = 0.2). In a second step, the RAMEB-P123 supramolecular assemblies were used as templates to direct the self-assembly of the pre-synthesised titania nanoparticles. This second step of synthesis was

performed at 25 °C because at this temperature, the RAMEB-P123 solutions present the lowest viscosity,[52] thus facilitating the structuration of the nanoparticles around the supramolecular template. After drying, the recovered xerogels were calcined at 500 °C to remove the organic template and allow further crystallisation of titania. The complete removal of the organic template was confirmed by ATR-FTIR spectroscopic analyses as noticed by the disappearance of the vibrational bands characteristic of the polymer and cyclodextrin (Fig. S2, ESI).

Fig. 2 displays the XRD patterns of the mesoporous titania prepared with a P123/Ti molar ratio of 0.027 (EO/Ti = 1) with increasing amounts of RAMEB (RAMEB/Ti molar ratio varying from 0 to 0.305) and calcined at 500 °C. The control sol-gel synthesised titania (*i.e.* prepared without template) is added for comparison.

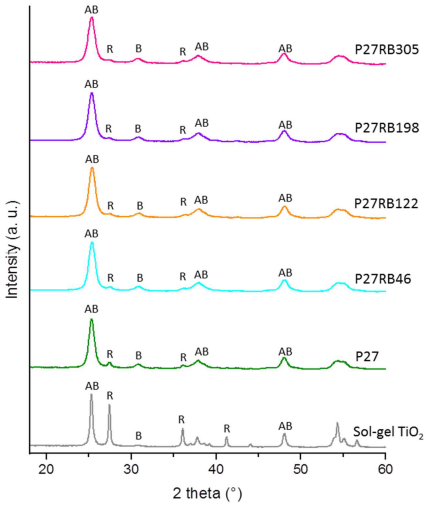

Fig. 2 XRD patterns of sol-gel titania prepared without template (sol-gel TiO_2), with Pluronic alone (P27) and with P123-RAMEB assemblies (P27RB46 to P27RB305). Samples were calcined at 500 °C. The "A", "B" and "R" in the figure denote the anatase, brookite and rutile phases respectively.

Before any thermal treatment, the sol-gel prepared titania nanoparticles contain 68 % anatase (A) (JCPDS card n° 00-021-1272) and 32 % brookite (B) (JCPDS card n° 01-076-1934) (Fig. S3, ESI). The crystallite sizes determined from the Scherrer formula are 6.6 ± 0.8 nm (A) and 5.3 ± 0.6 nm (B) owing to the high hydrolysis ratio employed in our synthesis which favours fast nucleation rates producing small and well-crystallised nanoparticles.[65,66] However, upon calcination at 500 °C, the small particles agglomerate and the increased degree of nanoparticle packing facilitates the phase transformation.[66] Therefore, from the diffraction diagram of the control TiO_2, one can note the appearance of an intense sharp peak at 2θ = 27.4° corresponding to the (110) plane of the rutile (R) (JCPDS card n° 00-034-0180), arising from the transformation of both anatase and brookite during calcination (Fig. 2). The contents of anatase and brookite, determined from the Rietveld refinement, drop to ~35 % and ~27 % respectively while ~38 % rutile form as a result of the sintering (Table 1). Meanwhile, the size of these three polymorphs grows to 36 nm (A), 19 nm (B) and 60 nm (R) as the phase transformation progresses. When the Pluronic alone is utilised as template (P27 sample), the rutile reflections remarkably decrease in intensity indicating a delay in the phase transformation. Interestingly, this phenomenon becomes even more pronounced upon addition of increasing amounts of RAMEB. Indeed, the diffraction peaks of anatase and brookite become broader indicating smaller crystallites, while more brookite forms and rutile polymorph almost disappears. Thus, for the P27RB198 sample, the size of the crystallites shrinks to 8-11 nm and the rutile content becomes negligible with respect to the contents of anatase (48 %) and brookite (52 %). Such anatase-to-brookite phase transformation upon addition of increasing amounts of organics has also been observed with another block copolymer (Pluronic F127) in a previous study[41] and has been explained by the fact that the fast combustion of the template during the heat treatment may direct the phase transformation towards the more dense structure of brookite (d = 4.12 g/cm^3 for brookite *vs.* 3.89 g/cm^3 for anatase).

To gain information about the impact of the template on the textural characteristics of titania, N_2-adsorption analyses were performed. All calcined samples display type IV isotherms which are typical features of mesoporous materials (Fig. 3).

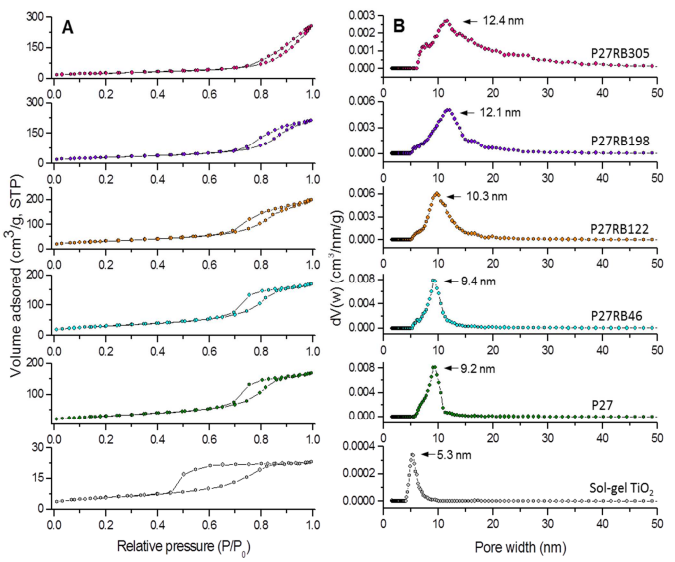

Fig. 3 N_2 adsorption isotherms (A) and corresponding pore size distribution plots (B) of sol-gel titania prepared without template (sol-gel TiO_2), with Pluronic alone (P27) and with P123-RAMEB assemblies (P27RB46 to P27RB305). Samples were calcined at 500 °C.

The control sol-gel titania presents a capillary condensation step that starts at a relative pressure (P/P_0) of about 0.4, indicating the presence of small mesopores with a diameter of 5.3 nm ascribed to the holes formed between the close packed crystallites. The addition of copolymer (P27 sample) strongly, but predictably,[41] improves the textural characteristics of the material, as shown by the steep rise in the nitrogen uptake at a

relative pressure $P/P_0 > 0.65$ and the abrupt increase in the pore size to 9.2 nm. Interestingly, when the cyclodextrin is added to the block copolymer solution, the textural characteristics are further improved. Therefore, for RAMEB/Ti molar ratios comprised between 0.046 and 0.198, the pore size increases progressively from 9.4 to 12.1 nm and the pore volume from 0.25 to 0.35 cm^3/g, while no notable evolution occurs above a RAMEB/Ti molar ratio of 0.198 (Table 1). Moreover, for the highest molar ratios employed, the isotherms become quite different in the region of relative pressures higher than 0.9 where the nitrogen adsorption continues to increase, indicating also the presence of some macropores.

From the representative FE-SEM images of the materials prepared without and with template (Fig. 4), the effect of the supramolecular assemblies on the morphology of the network can be clearly visualised.

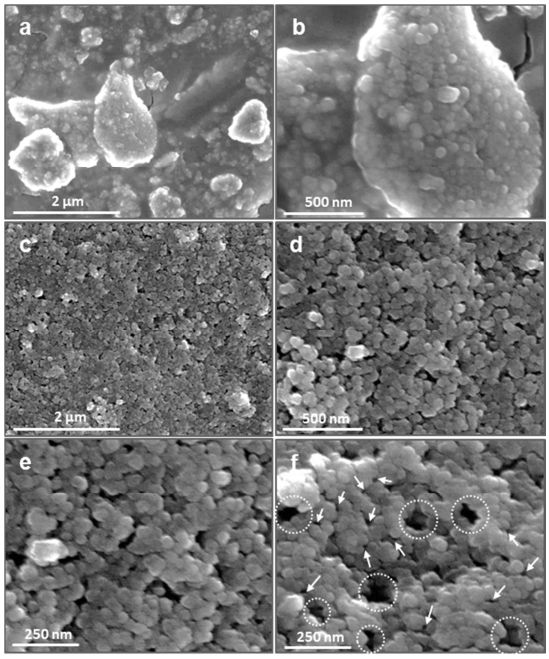

Fig. 4 Representative FE-SEM images taken at different magnifications for sol-gel titania prepared without template (a, b) and for titania prepared with P123-RAMEB assemblies (P27RB198 sample) (c-f). Samples were calcined at 500 °C.

Therefore, it can be seen that the sol-gel titania prepared without template is comprised of rounded particles densely packed into large aggregates with no regular shape and very low interparticle porosity (Fig. 4 a, b). In contrast, the material prepared using the supramolecular assemblies (P27RB198 sample) shows uniform particles with spherical shape indicating the important role of the template in restructuring the particle network (Fig. 4 c-f). Moreover, several voids are also noticed at a high yield creating a network of interconnected mesopores with an average diameter of 10-20 nm (see arrows) and macropores with an average diameter of 60-100 nm (see dotted circles), in accordance with the shape of the N_2-adsorption isotherm at high relative pressures. This indicates that the material has adopted some characteristics of the supramolecular template maintaining a nanostructured network even after calcination at 500 °C.

Further evidence for the effect of the supramolecular assemblies on the crystal phase composition was provided from UV-visible absorption spectroscopy (Fig. 5). Thus, the energy gap (E_g) of the control sol-gel TiO_2, calculated from the extrapolation of the absorption edge into the energy axes (409 nm), is found to be 3.03 eV. This value is very close to the E_g of rutile (3.02 eV)[67] which is the predominant polymorph in this sample (38 % (R) *vs.* 35 % (A) and 27 % (B)) (Fig. 2, Table 1). On the other hand, the spectra of the samples prepared with Pluronic P123 and RAMEB-P123 assemblies present a clear blue shift of the absorption edge towards shorter wavelengths. Note that the value of the band gap depends on the formulation of the template. Indeed, for the P27, P27RB46 and P27RB122 samples, which contain *ca.* 50-55% anatase, the extrapolation of the absorption edge yields band gap values in the range of 3.16-3.20 eV, whereas for the P27RB198 and P27RB305 samples, which contain *ca.* 52-54 % brookite and almost no rutile, the band gap increases to 3.29 eV. Although few experimental data are available in literature for pure brookite, several authors agree that its band gap is *ca.* 3.3 eV, higher than that of anatase and rutile.[25,68] The relatively larger band gap values observed for the highest RAMEB/Ti molar ratios corroborate well with the major influence of brookite as predominant polymorph, consistent with our XRD data (Fig. 2, Table 1). Additionally, the quantum effects, which are usually produced in confined regions with semi-conductor particles having at least one dimension in the range of 1-10 nm, are also presumed to contribute to the observed effects.[69]

Taken together, our XRD, N_2-adsorption, FE-SEM and UV-visible results provide clear evidence of the fact that the supramolecular assemblies formed between the randomly methylated β-CD and Pluronic P123 act as efficient templates for tuning the crystal properties of titania as well as for controlling its porosity, in agreement with the synthesis pathway illustrated in Fig. 1.

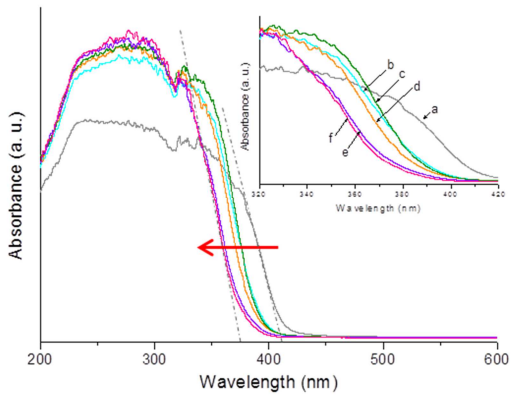

Fig. 5 UV-vis spectra and zoomed-in plot from 320 to 420 nm (inset) of sol-gel titania prepared without template (a), with Pluronic alone (b), and with P123-RAMEB assemblies: P27RB46 (c), P27RB122 (d), P27RB198 (e), P27RB305 (f). Samples were calcined at 500 °C. The arrow is drawn as a guide to the eye.

3.2 Effect of the calcination temperature

The transformation sequence among the three titania polymorphs is size dependent.[36,70] In bulk, rutile is the only thermodynamically stable phase, while bulk anatase and bulk brookite are metastable. However, at the nanoscale, for particles with diameters below *ca.* 14 nm, anatase is more stable than rutile.[36] Theoretical calculations (DFT) explain that the reversal of the stability in TiO_2 nanoparticles relative to the bulk phase is due to the lower surface energy in anatase compared to that in rutile at the nanoscale.[71] Such difference in the surface energy also explains why anatase can be readily synthesised at ultrafine sizes under ambient conditions. However, upon heating, the crystal growth leads to an alteration of phase stabilities and ultimately to the conversion of both anatase and brookite to rutile.[70] In addition, calorimetric measurements confirm that rutile has the highest surface enthalpy (2.2 ± 0.2 J/m^2), followed by brookite (1.0 ± 0.2 J/m^2) and anatase (0.4 ± 0.1 J/m^2).[72] This suggests that as the crystallites grow up, anatase would first transform to rutile or brookite before brookite transforms to rutile. The mechanism of phase transformation in titania has also been reported to be a process of nucleation and growth depending strongly on the agglomeration state of the particles.[73,74] Indeed, when the anatase particles are in intimate contact with each other, the interfaces of the contacting grains provide the nucleation sites of the rutile phase. Once the nucleation is initiated, the phase transformation quickly spreads throughout the whole agglomerated particles until the complete transformation of anatase and/or brookite to rutile is completed.

To follow the sequence of phase transformation in our titania materials prepared using the supramolecular assemblies, the sample presenting the best characteristics (P27RB198) was calcined at different temperatures ranging between 400 and 800 °C. From the XRD patterns shown in Fig. 6, it can be noticed that at 400 °C, anatase is the dominant polymorph. Thus, the initial phase contents determined from Rietveld refinements are 90% (A) and 10% (B) and the crystallite sizes obtained from the Scherrer formula are 9.0 nm (A) and 4.4 nm (B) (Table 1). At 500 °C, anatase transforms rapidly to brookite, as can be seen from the increase in the intensity of the (121) diffraction peak located at 30.8°, while the nucleation of the rutile polymorph has just begun (only 1% of rutile is detected at 500 °C). However, upon heating to 600 °C, the particle coarsening induces a significant increase in the crystallite size and rutile content up to 23.6 nm and 17% respectively, while simultaneously, the brookite content drops from 52 to 35%. Once the rutile crystallites are formed, they grow very rapidly. Therefore, for a calcination temperature of 700 °C, the diffraction peaks of anatase and brookite gradually diminish in intensity and rutile becomes the predominant polymorph (62 %). Finally, at 800 °C, the fast particle coarsening leads to the whole transformation of the remaining anatase to rutile which is the thermodynamically stable polymorph in this bigger particle size range (> 60 nm).

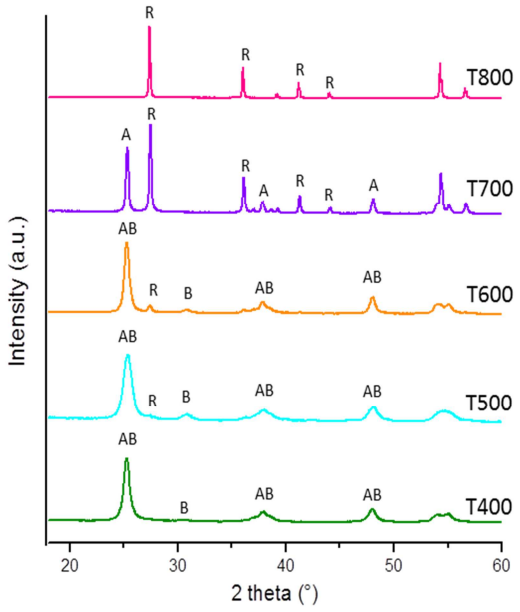

Fig. 6 XRD patterns of the P27RB198 titania calcined at different temperatures: 400 °C (16 h), 500 °C (2 h), 600 °C (2 h), 700 °C (2 h) and 800 °C (2 h).

Overall, our results indicate that at lower temperatures (400-500 °C), the initial process involves the transformation of anatase to brookite. Although anatase is likely to be thermodynamically stable in this size range (< 11 nm), the fast combustion of the organic template seems to direct the transformation sequence toward the densest polymorph, *i.e.* the brookite. For a higher calcination temperature (600 °C), brookite starts transforming to rutile followed by the conversion at 700-800 °C of both anatase and brookite to rutile, in agreement with the theoretical predictions of Zhang and Banfield.[70]

By comparing the evolution of the phase transformation in the sol-gel and P27RB198 titania materials, it is clearly noticed that the supramolecular assemblies play a key role in inhibiting the crystal growth and stabilising the anatase and brookite polymorphs with respect to the rutile. Thus, for the sol-gel titania prepared without template, both anatase and brookite are completely transformed to rutile already at 600 °C (Fig S4, ESI). Such a fast phase transformation can be attributed to the small size of the crystallites in the starting material (6.6 nm for anatase and 5.3 nm for brookite) as well as to their high level of aggregation which facilitate the contact between neighbouring grains, thus resulting in a very rapid conversion to rutile. On the other hand, for the P27RB198 titania material, the complete transformation of anatase and brookite to rutile is detected at a much higher calcination temperature, *i.e.* 800 °C (Fig. 6). This behaviour may be explained by the fact that when the TiO_2 nanocrystals self-assemble around the organic template, the reduced degree of nanoparticle packing provides less contact sites between neighbouring grains, thus delaying the rutile nucleation.

The calcination temperature has also a strong impact on the textural characteristics of the titania materials, as can be noticed from the N_2 adsorption isotherms shown in Fig. 7. Therefore, the P27RB198 sample calcined at 400 °C presents the best characteristics with a surface area of 158 m^2/g, a pore volume of 0.45 cm^3/g and a pore size of 9.3 nm (Table 1). A slight alteration of these characteristics is noticed at 500 °C due to the size of the crystallites which just starts to increase (8-11 nm) while the rutile content is still negligible (1%). More pronounced changes are observed for the materials calcined at 600 and 700 °C for which the growth of the rutile grains provokes a fast decrease in the surface area and pore volume. Therefore, for a calcination temperature of 700 °C, the surface area drops to 16 m^2/g and the pore volume to 0.14 cm^3/g while the pore size distribution becomes very broad, indicating the beginning of the collapse of the titania network, consistent also with the abrupt increase in the crystallite size of the rutile up to *ca.* 63 nm (Table 1).

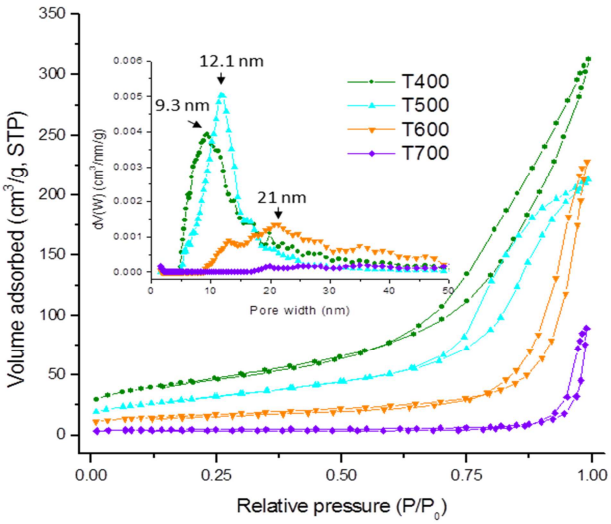

Fig. 7 N_2 adsorption isotherms and corresponding PSD (inset) of the P27RB198 titania calcined at different temperatures from 400 to 700 °C.

The changes observed in particle size and phase content are also confirmed by UV-Vis spectroscopy (Fig. 8). Indeed, with increasing the calcination temperature, the spectra of the P27RB198 material show a red shift of the absorption edge toward longer wavelengths, consistent with the increase in the crystallite size. Moreover, the shift of the band gap for the material calcined at 800 °C to *ca.* 3.03 eV, close to the band gap of the rutile, matches well with our XRD results shown in Fig. 6 where the onset temperature of the anatase-to-rutile transformation is located between 700 and 800 °C.

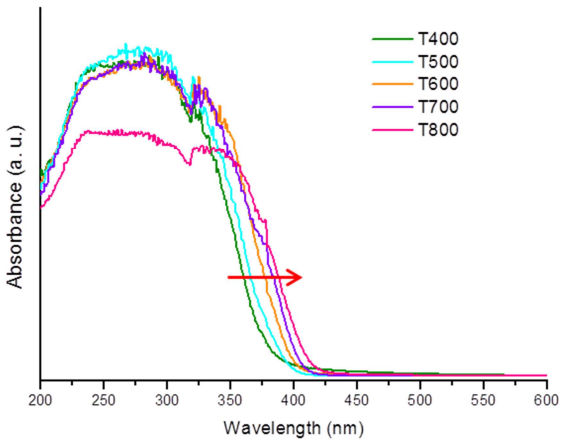

Fig. 8 UV-vis spectra of the P27RB198 titania material calcined at different temperatures from 400 to 800 °C. The arrow is drawn as a guide to the eye.

3.3 Photocatalytic activity

Phenoxyacetic acid (PAA) is a parent molecule of the well-known herbicides like 2,4-dichlorophenoxyacetic acid (2,4-D) and 2,4,5-trichlorophenoxyacetic acid (2,4,5-T) which are highly toxic compounds.[75,76] In this study, PAA was chosen as representative pollutant to evaluate the photocatalytic activity of mesoporous titania prepared using the different templates.

In Fig. 9, we present the PAA photodegradation rate obtained after 7 hours of exposure under UV-light illumination (360 nm). We note that the photocatalytic activity of the catalyst is significantly affected by the nature of the template. Thus, when the Pluronic alone is utilised as template (P27 sample), a sharp increase in the photodegradation rate from 43% (control sol-gel titania) to 75% occurs. Interestingly, upon addition of increasing amounts of RAMEB, the photodegradation rate progressively increases reaching a maximum photocatalytic conversion rate of 88% for the P27RB198 sample.

In our view, the origin of the enhancement in the photocatalytic activity of titania should result from a combined effect of improved textural characteristics and controlled crystalline properties of the catalyst which, in turn, depend on the nature of the template. Indeed, the high surface area obtained for the P27RB198 titania material (110 m^2/g), which may be correlated to the lower crystallite size in this sample (8-16 nm), should provide a larger number of adsorption sites and active centres surrounding the electron-hole pairs, thus facilitating the first step of the photocatalytic reaction. On the other hand, the high pore volume (0.35 cm^3/g) may allow for more PAA to be adsorbed on the internal surface of the pores, thus improving the diffusion of the substrate to the adsorption sites during the photocatalytic process. Finally, the low density of crystalline defects obtained for the material calcined at 500 °C may produce less grain boundaries and thus, a larger amount of charge carriers should reach the surface of the crystal to initiate the redox reactions.

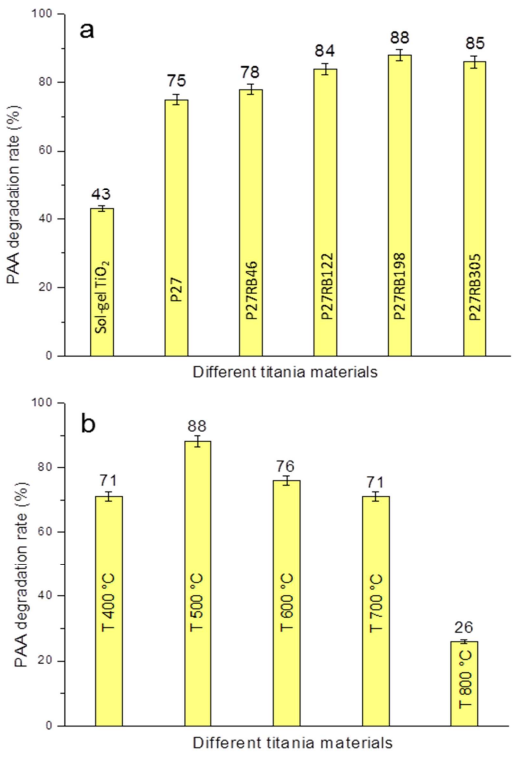

Fig. 9 Photocatalytic degradation rate of the different titania materials prepared by using the P123-RAMEB supramolecular assemblies as templates (a) and of the P27RB198 catalyst calcined at different temperatures (b).

It is worth emphasising that the combination of good structural and textural properties requires the choice of a correct temperature of calcination. For instance, the P27RB198 material calcined at 400 °C presents better textural characteristics (S_{BET} = 158 m^2/g; pv = 0.45 cm^3/g; ps = 9.3 nm) compared to the material calcined at 500 °C (S_{BET} = 110 m^2/g; pv = 0.35 cm^3/g; ps = 12.1 nm) (Fig. 7 and Table 1), but the high density of defects at 400 °C should favour the electron-hole recombination, thus resulting in low degradation rates. Conversely, above 500 °C, the catalyst is well-crystallised but now, the size of the crystallites increases very rapidly (cs for rutile = 62.5 nm at 700 °C) resulting in a degradation of the textural characteristics (S_{BET} = 16 m^2/g; pv = 0.14 cm^3/g at 700 °C). So, the temperature of 500 °C chosen for our calcinations represents the conditions under which an optimal balance of high pore volumes, large surface areas and high crystallinity may be obtained to achieve the optimum photocatalyst for the photodegradation of PAA in water.

Conclusions

In this work, we investigated the possibility of utilising the supramolecular assemblies formed between the block copolymer P123 and the randomly methylated β cyclodextrin as templates for the synthesis of a series of mesoporous titania material with controlled porosity and crystalline framework. As reported previously, the addition of increasing amounts of randomly methylated β-CD promoted a progressive growth of the Pluronic micelles which was manifested by a marked enhancement in the pore size, pore volume and surface area of titania as well as a higher stability of the anatase and brookite polymorphs with respect to the rutile. The utilisation of controlled amounts of cyclodextrin also allowed for fine-tuning the phase composition and crystallite size while promoting the formation of particles with a spherical shape. The stability of these materials was attributed to the ability of the supramolecular assemblies to reduce the number of contact sites between neighbouring grains, therefore inhibiting the nucleation of the rutile phase. Finally, the mesoporous titania materials prepared using the P123-RAMEB assemblies as template were shown to efficiently catalyse the photodegradation of the phenoxyacetic acid in water, giving rise to higher conversion rates compared to the sol-gel titania particles. Overall, our results revealed that knowledge about the interactions of these cyclic oligosaccharides with the block copolymer and with titania colloids is fundamental for understanding and controlling the properties of the resultant photocatalyst. Combining these findings with the well-known ability of the cyclodextrins to selectively bind a variety of metal complexes and form supramolecular host-guest adducts may open up wide opportunities for designing nanostructured metal-capped photocatalysts for energy and environmental challenges.

Acknowledgements

The European Regional Development Fund (ERDF), the Conseil Regional du Nord-Pas de Calais, the CNRS and the Ministère de l'Education Nationale de l'Enseignement Supérieur et de la Recherche are acknowledged for funding of the X-ray diffractometer. A. Lannoy is grateful to the Region Nord Pas-de-Calais and University of Artois for the PhD grant support. The laboratory participates in the Institut de Recherche en ENvironnement Industriel (IRENI), which is financed by the Communauté Urbaine de Dunkerque, the Région Nord Pas-de-Calais, the Ministère de l'Enseignement Supérieur et de la Recherche, the CNRS and the ERDF. We thank Laurence Burylo (UCCS, University of Lille) and Nicolas Kania (UCCS, University of Artois) for technical assistance in XRD measurements and photocatalytic measurements respectively. Antonio Da Costa (UCCS, University of Artois) and Nora Djelal (UCCS, University of Lille) are acknowledged for their help with FE-SEM analyses.

Notes and references

[a] *Université d'Artois, UCCS, UMR-CNRS 8181, Faculté des Sciences Jean Perrin, Rue Jean Souvraz, SP 18, F-62307 Lens, France. E-mail : rudina.bleta@univ-artois.fr*

† Electronic Supplementary Information (ESI) available: Fig. S1: XRD patterns resulting from pattern matching and Rietveld refinements. Fig. S2: ATR-FTIR spectra. Fig. S3: XRD pattern of the sol-gel TiO_2 xerogel and its structural and textural characteristics (Table S1). Fig. S4: XRD pattern of the sol-gel TiO_2 at 600 °C.

Table 1. Structural and textural parameters of the different mesoporous titania materials prepared through template-directed colloidal self-assembly.

Sample			Anatase		Brookite		Rutile		N_2 adsorption			UV-Vis
			cs^c (nm)	ct^d (%)	cs^c (nm)	ct^d (%)	cs^c (nm)	ct^d (%)	$S_{BET}{}^e$ (m^2/g)	pv^f (cm^3/g)	ps^g (nm)	$E_g{}^h$ (eV)
	P+RB/Ti[a]	RB/P[b]	Effect of addition of P123-RAMEB assemblies									
Sol-gel TiO_2	-		36.4±2.9	35.3±2.8	18.7±1.5	26.5±2.1	60.4±4.8	38.2±3.1	21±1	0.03±0.00	5.3±1.1	3.03
P27	0.027	0	17.2±1.4	54.5±4.4	13.8±1.1	42.1±3.4	20.8±1.7	3.4±0.3	89±4	0.24±0.01	9.2±1.8	3.16
P27RB46	0.073	1.7	15.5±1.2	51.5±4.1	11.6±0.9	46.0±3.7	16.6±1.3	2.5±0.2	109±5	0.25±0.01	9.4±1.9	3.16
P27RB122	0.149	4.5	13.6±1.1	50.1±4.0	8.9±0.7	48.6±3.9	13.4±1.1	1.3±0.1	112±6	0.29±0.01	10.3±2.1	3.20
P27RB198	0.225	7.4	10.8±0.9	47.7±3.8	7.6±0.6	51.5±4.1	10.7±0.9	0.8±0.1	110±6	0.35±0.02	12.1±2.4	3.29
P27RB305	0.332	11.4	9.9±0.8	45.4±3.6	6.7±0.5	54.3±4.3	9.0±0.7	0.3±0.1	96±5	0.36±0.02	12.4±2.5	3.29
			Effect of the calcination temperature (P27RB198 sample)									
T400	0.225	7.4	9.0±0.7	90.4±7.2	4.4±0.4	9.6±0.8	-	-	158±8	0.45±0.02	9.3±1.9	3.30
T500	0.225	7.4	10.8±0.9	47.7±3.8	7.6±0.6	51.5±4.1	10.7±0.9	0.8±0.1	110±6	0.35±0.02	12.1±2.4	3.29
T600	0.225	7.4	17.7±1.4	48.1±3.8	8.5±0.7	35.2±2.8	23.6±1.9	16.7±1.3	58±3	0.35±0.02	21.0±4.2	3.15
T700	0.225	7.4	35.2±2.8	37.6±3.0	-	-	62.5±5.0	62.4±5.0	16±1	0.14±0.01	-	3.07
T800	0.225	7.4	-	-	-	-	82.8±6.6	100	-	-	-	3.03

[a](P123+RAMEB)/Ti molar ratio in the sol, [b]RAMEB/P123 molar ratio in the sol, [c]crystallite size calculated from the Scherrer formula, [d]polymorph content determined from Rietveld refinements, [e]specific surface area determined by BET method in the relative pressure range of 0.1-0.25, [f]pore volume computed by NLDFT, [g]pore size determined by NLDFT, [h]band gap energies (E_g) calculated using the equation $E_g = (1239/\lambda)$ eV.

References

[1] G. M. Whitesides and B. Grzybowski, *Science*, 2002, **295**, 2418-2421.
[2] S. Mann, *Nature Materials*, 2009, **8**, 781.
[3] T. Sun and J. Y. Ying, *Nature*, 1997, **389**, 704.
[4] C. T. Kresge, M. E. Leonowicz, W. J. Roth, J. C. Vartuli and J. S. Beck, *Nature*, 1992, **359**, 710.
[5] J. S. Beck, J. C. Vartuli, W. J. Roth, M. E. Leonowicz, C. T. Kresge, K.D. Schmitt, C. T.-W. Chu, D. H. Olson, E. W. Sheppard, S. B. McCullen, J. B. Higgins and J. L. Schlenker, *J. Am. Chem. Soc.*, 1992, **114**, 10834.
[6] B. L. Su, C. Sanchez, X. Y. Yang: Hierarchically structured porous materials. From nanoscience to catalysis, separation, optics, energy, and life science. In: B. L. Su, C. Sanchez and X. Y. Yang (eds.) Wiley-VCH Verlag GmbH, Weinheim (2012).
[7] G. Ozin, *Chem. Commun.*, 2000, 419.
[8] Y. Hwang, K. Lee and Y. Kwon, *Chem. Commun*., 2001, 1738.
[9] M. Wong, E. Jeng and J. Ying, *Nano Lett*., 2001, **1**, 637.
[10] A. L. Rogach, D. V. Talapin, E. V. Shevchenko, A. Kornowski, M. Haase and H. Weller, *Adv. Funct. Mater.*, 2002, **12**, 653.
[11] H. Zhang, E. W. Edwards, D. Wang and H. Möhwald, *Phys. Chem. Chem. Phys*., 2006, **8**, 3288.
[12] R. Bleta, P. Alphonse, L. Pin, M. Gressier and M. J. Menu, *J. Colloid Interface Sci.*, 2012, **367**, 120.
[13] G. Kaune, M. Memesa, R. Meier, M. A. Ruderer, A. Diethert, S. V. Roth, M. D'Acunzi, J. S. Gutmann, and P. Mueller-Buschbaum, *ACS Appl. Mater. Interfaces*, 2009, **1**, 2862.
[14] D. Chen and R. A. Caruso, *Adv. Funct. Mater*., 2013, **23**, 1356-1374.
[15] W. Zhao, W. Ma, C. Chen, J. Zhao and Z. Shuai, *J. Am. Chem. Soc*., 2004, **126**, 4782.
[16] L. Gomathi Devi and R. Kavitha, *Appl. Catal. B Environ*., 2013, **140-141**, 559.
[17] A. Fujishima and K. Honda, *Nature*, 1972, **238**, 37.
[18] S. U. M. Khan, M. Al-Shahry and W. B. Ingler, *Science*, 2002, **297**, 2243.
[19] M. Ni, M. K. H. Leung, D. Y. C. Leung and K. A. Sumathy, *Renewable Sustainable Energy Rev.*, 2007, **11**, 401.
[20] S. C. Pillai, P. Periyat, R. George, J. Colreavy, R. George, H. Hayden, M. Seery, D. E. McCormack, D. Corr and S. J. Hinder, *J. Phys. Chem. C*, 2007, **111**, 1605.
[21] P. Periyat, S. C. Pillai, D. E. McCormack, J. Colreavy and S. J. Hinder, *J. Phys. Chem. C*, 2008, **112**, 7644.

[22] A. R. Gandhe, S. P. Naik and J. B. Fernandez, *Microporous Mesopourous Mater*., 2005, **87**, 103.
[23] B. Ohtani, J. Handa, S. Nishimoto and T. Kagiya, *Chem. Phys. Lett*., 1985, **120**, 292.
[24] J. G. Li, T. Ishigaki and X. D. Sun, *J. Phys. Chem*., 2007, **111**, 4969.
[25] Q. Tay, X. Liu, Y. Tang, Z. Jiang, T. Chien Sum and Z. Chen, *J. Phys. Chem. C*, 2013, **117**, 14973.
[26] J. C. Yu, L. Z. Zhang and J. G. Yu, *Chem. Mater*., 2002, **14**, 4647.
[27] G. Tian, H. Fu, L. Jing, B. Xin and K. Pan, *J. Phys. Chem. C*, 2008, **112**, 3083.
[28] R. Boppella, P. Basak and S. V. Manorama, *Appl. Mater. Interfaces*, 2012, **4**, 1239.
[29] A. L. Linsebigler, G. Q. Lu and J. T. Yates, *Chem. Rev*., 1995, **95**, 735.
[30] J. Ovenstone, *J. Mater. Sci.*, 2001, **36**, 1325.
[31] S. Y. Choi, M. Mamak, N. Coombs, N. Chopra and G. A**.** Ozin, *Adv. Funct. Mater*., 2004, **14**, 335.
[32] H. G. Yang, C. H. Sun, S. Z. Qiao, J. Zou, G. Liu, S. C. Smith, H. M. Cheng and G. Q. Lu, *Nature*, 2008, **453**, 638.
[33] J. Ryu and W. Choi, *Environ. Sci. Technol.*, 2008, **42**, 294.
[34] X. Wang, M. Blackford, K. Prince and R. A. Caruso, *ACS Appl. Mater. Interfaces*, 2012, **4**, 476.
[35] X. Wang, L. Cao, D. Chen and R. A. Caruso, *ACS Appl. Mater. Interfaces*, 2013, **5,** 9421.
[36] H. Zhang and J. F. Banfield, *J. Mater. Chem.*, 1998, **8**, 2073.
[37] D. J. Reidy, J. D. Holmes and M. A. Morris, *J. Eur. Ceram. Soc*., 2006, **26**, 1527.
[38] A. Navrotsky and O. J. Kleppla, *J. Am. Ceram. Soc.*, 1967, **50**, 626.
[39] P. Yang, D. Zhao, D. Margolese, B. Chmelka and G. Stucky, *Nature*, 1998, **396**, 152.
[40] P. Yang, D. Zhao, D. Margolese, B. Chmelka and G. Stucky, *Chem. Mater*., 1999, **11**, 2813.
[41] R. Bleta, P. Alphonse and L. Lorenzato, *J. Phys. Chem. C*, 2010**, 114**, 2039.
[42] D. L. Li, H. S. Zhou and I. Honma, *Nat. Mater*., 2004, **3**, 65.
[43] A. Karthikeyan and R. M. Almeida, *J. Non-Cryst. Solids*, 2000, **274**, 169.
[44] M. Marszewski and M. Jaroniec, *Langmuir*, 2013, **29**, 12549.
[45] J. Szejtli, *Chem. Rev.*, 1998, **98**, 1743.
[46] R. Breslow and S. D. Dong, *Chem. Rev.*, 1998, **98**, 1997.
[47] S. Polarz, B. Smarsly, L. Bronstein and M. Antonietti, *Angew. Chem., Int. Ed.*, 2001, **40**, 4417.
[48] B. H. Han and M. Antonietti, *Chem. Mater*., 2002, **14**, 3477.
[49] B. H. Han, B. Smarsly, C. Gruber and G. Wenz, *Microporous Mesoporous Mater.*, 2003, **66**, 127.
[50] R. Bleta, S. Menuel, B. Léger, A. Da Costa, E. Monflier and A. Ponchel, *RSC Adv.*, 2014, **4**, 8200.
[51] R. Bleta, C. Machut, B. Léger, E. Monflier and A. Ponchel, *Macromolecules*, 2013, **46**, 5672.
[52] R. Bleta, C. Machut, B. Léger, E. Monflier and A. Ponchel, *J. Incl. Phenom. Macrocycl. Chem.*, 2014 DOI 10.1007/s10847-014-0405-7.
[53] J. Y. Zheng, J. B. Pang, K. Y. Qiu and Y. Wei, *J. Mater. Chem*., 2001, **11**, 3367.
[54] J. W. Chung and S. Y. Kwak, Patent, WO 2008066229 A1, 2008.
[55] E. K. Arnold and V. R. Beasley, *Vet. Hum. Toxicol.*, 1989, **31**, 121.
[56] C. Timchalk, *Toxicology*, 2004, **200**, 1.
[57] P. Alphonse, R. Bleta and R. Soules, *J. Colloid Interface Sci.*, 2009, **337**, 81.
[58] J. Rodriguez-Carvajal, FULLPROF: A Program for Rietveld Refinement and Pattern Matching Analysis. In Abstracts of the Satellite Meeting on Powder Diffraction of the XV Congress of the IUCR, Toulouse, France; International Union of Crystallography: Chester, U.K., 1990; 127.
[59] T. Roisnel and J. Rodriguez-Carvajal, WinPLOTR [June 2005] A Windows Tool for Powder Diffraction Pattern Analysis. In Materials Science Forum, Proceedings of the 7th European Powder Diffraction Conference (EPDIC 7); Delhez, R., Mittenmeijer, E. J., Eds.; Trans Tech Publications: Zurich, Switzerland, 2000, 118.
[60] P. Scherrer, *Nachr. Ges. Wiss. Göttingen Math.-Phys. Kl.*, 1918, **2**, 98.
[61] S. Brunauer, P. H. Emmett and E. Teller, *J. Am. Chem. Soc.*, 1938, **60**, 309.
[62] R. Evans, U. M. B. Marconi and P. Tarzona, *J. Chem. Soc. Faraday Trans. II*, 1986, **82**, 1763.
[63] E. K. Arnold and V. R. Beasley, *Vet. Hum. Toxicol.*, 1989, **31**, 121.
[64] C. Timchalk, *Toxicology*, 2004, **200 (1)**, 1.
[65] B. L. Bischoff and M. A. Anderson, *Chem. Mater*. 1995, **7**, 1772.
[66] K. Yanagisawa and J. Ovenstone, *J. Phys. Chem. B* 1999, **103**, 7781.
[67] M. R. Hoffmann, S. T. Martin, W. Choi and D. W. Bahnemann, *Chem. Rev.*, 1995, **95**, 69.
[68] Y. Dongjiang, L. Hongwei, Z. Zhanfeng, Y. Yong, Z. Jin-Cai, E. R. Waclawik, K. Xuebin and Z. Huaiyong, *J. Am. Chem. Soc.*, 2009, **131**, 17885.
[69] L. Brus, *J. Phys. Chem.*, 1986, **90**, 2555.
[70] H. Z. Zhang and J. F. J. Banfield, *Phys. Chem. B*, 2000, **104**, 3481.
[71] D. R. Hummer, J. D. Kubicki, P. R. C. Kent, J. E. Post and P. J. Heaney, *J. Phys. Chem. C*, 2009, **113**, 4240.
[72] M. R. Ranade, A. Navrotsky, H. Z. Zhang, J. F. Banfield, S. H. Elder, A. Zaban, P. H. Borse, S. K. Kulkarni, G. S. Doran and H. J. Whitfield, *Proc. Natl. Acad. Sci. U.S.A*. 2002, **99**, 6476.
[73] J. Zhang, M. Li, Z. Feng, J. Chen and C. Li, *J. Phys. Chem. B*, 2006, **110**, 927.
[74] J. Zhang, Q. Xu, M. Li, Z. Feng, and C. Li, *J. Phys. Chem. C*, 2009, **113**, 1698.
[75] S. P. Kamble, S. B. Sawant and V. G. Pangarkar, *Chem. Eng. Res. Des.*, 2006, **84**, 355.
[76] H. K. Singh, M. Saquib, M. M. Haque, M. Muneer and D. W. Bahnemann, *J. Mol. Catal. A: Chem*., 2007, **264**, 66.

